


Cite this: *RSC Adv.*, 2022, 12, 26463

RamanNet: a lightweight convolutional neural network for bacterial identification based on Raman spectra

Bo Zhou, ^{ab} Yu-Kai Tong, ^b Ru Zhang^{*a} and Anpei Ye^{*b}

Raman spectroscopy combined convolutional neural network (CNN) enables rapid and accurate identification of the species of bacteria. However, the existing CNN requires a complex hyperparameters model design. Herein, we propose a new simple network architecture with less hyperparameter design and low computation cost, RamanNet, for rapid and accurate identifying of bacteria at the species level based on its Raman spectra. We verified that compared with the previous CNN methods, the RamanNet reached comparable results on the Bacteria-ID Raman spectral dataset and PKU-bacterial Raman spectral datasets, but using only about 1/45 and 1/297 network parameters, respectively. RamanNet achieved an average isolate-level accuracy of $84.7 \pm 0.3\%$, antibiotic treatment identification accuracy of $97.1 \pm 0.3\%$, and distinguished accuracy of $81.6 \pm 0.9\%$ for methicillin-resistant and -susceptible *Staphylococcus aureus* (MRSA and MSSA) on the Bacteria-ID dataset, respectively. Moreover, it achieved an average accuracy of 96.04% on the PKU-bacterial dataset. The RamanNet model benefited from fewer model parameters that can be quickly trained even using CPU. Therefore, our method has the potential to rapidly and accurately identify bacterial species based on their Raman spectra and can be easily extended to other classification tasks based on Raman spectra.

Received 16th June 2022
Accepted 25th August 2022

DOI: 10.1039/d2ra03722j

rsc.li/rsc-advances

1. Introduction

Rapid and accurate identification of pathogenic bacteria is critical in hospitals and epidemic situations. Nucleic acid assays and immunological methods are common methods for identifying bacteria. Among them, the widely used methods are enzyme-linked immunosorbent assay (ELISA)^{1,2} and polymerase chain reaction (PCR),³ which have high sensitivity and specificity. However, these methods require complex sample pre-treatment, expensive reagents, time-consuming bacterial culture, and DNA/RNA amplification. Also, some bacteria are difficult to grow under laboratory conditions. Matrix-assisted laser desorption/ionization time-of-flight mass spectrometry (MALDI-TOF)⁴⁻⁶ is another rapidly developing technology that can identify bacteria by their peptide mass fingerprints. Although the above methods are well developed and trusted, extracting protein, RNA, or DNA is destructive to cells, limiting further multimodal analysis for the same cell. Therefore, a rapid and non-destructive bacterial identification strategy is needed.

Raman spectroscopy enables the identification of bacteria in a fast, non-destructive and label-free manner.⁷⁻¹¹ The technology allows for the analysis of the molecular structure and

chemical composition of substances, thus leading to significant progress in classifying components of complex mixtures.^{12,13} Different components in bacterial cells will produce unique spectral fingerprints on Raman spectra, and we can identify different bacteria based on these unique Raman fingerprints. Overall, Raman spectroscopy has significant potential to identify bacteria at the species level or the level of antibiotic resistance.^{10,14} In recent years, the use of neural networks to automatically feature Raman spectra has significantly improved the identification accuracy of pathogenic bacteria compared to traditional machine learning algorithms.^{8,9,15}

To improve the classification accuracy of convolutional neural network (CNN) for bacterial Raman spectra, many attempts have focused on using dozens of filters,^{14,16-18} increasing the depth of the network,^{14,16} and adopting more advanced classification algorithm models, which were mainly used in the optimization methods of the image classification field. These methods often result in longer training times and more complex hyperparameter designs for neural networks. However, a common but significant problem has not been resolved, that is, the existing CNN is not explicitly designed for Raman spectra data, so we may not fully exploit the advantages of CNNs. In previous studies, state-of-the-art CNN techniques from image classification, such as residual network (ResNet), were used to classify low signal-to-noise ratio (SNR) Raman spectra data.¹⁴ Ho *et al.* used dozens of filters in the 26-layer CNN to achieve average isolate-level accuracies exceeding 82%.

^aSchool of Science, Beijing University of Posts and Telecommunications, Beijing 100876, China. E-mail: ruzhang@bupt.edu.cn

^bKey Laboratory for the Physics and Chemistry of Nanodevices, School of Electronics, Peking University, Beijing 100871, China. E-mail: yap@pku.edu.cn



Maruthamuthu. *et al.*¹⁶ classified 12 microbes Raman spectra with an accuracy exceeding 95% using 18-layers ResNet with hundreds of filters in each layer. Liu *et al.*²⁰ explored the rapid identification of 13 microorganisms by single-cell Raman spectroscopy (scRS) and achieved an average accuracy of $88.5 \pm 4\%$ using a 3-layers one-dimensional convolutional neural network (1DCNN) with dozens of convolution kernels. In fact, Raman spectra, as one-dimensional sequences without depth, are much simpler than images (multi-dimensional matrices). Therefore, such a complex network structure may not be required for identifying bacterial Raman spectroscopy at species-level accuracy. Through extensive experiments, we demonstrated that for bacterial Raman spectra, two or three convolutional layers with one filter per convolutional layer in a CNN are sufficient to achieve fast and high accurate identification at the species-level.

Herein, we proposed a novel and simple CNN model named RamanNet for rapid and accurate identifying bacteria at the species-level based on bacterial scRS. The RamanNet consists of an initial convolution layer followed by two residual layers, a flatten layer, and a final fully classification layer, and each convolutional layer contains only one filter. We validated the performance of RamanNet on both the Bacteria-ID dataset and PKU-bacterial dataset. RamanNet achieved an average isolate-level accuracy of $84.7 \pm 0.3\%$ and an accuracy of antibiotic treatment identification of $97.1 \pm 0.3\%$ on the Bacteria-ID dataset. Moreover, RamanNet has 296.9 times fewer parameters compared with ResNet but achieved a comparable classification accuracy of 96.04% on the PKU-bacterial dataset. Due to the optimization of the RamanNet structure, we can rapidly train the model using only CPU rather than GPU. We believe this research would provide guidance and reference for bacterial Raman spectral analysis using convolutional neural networks.

2. Materials and methods

First, we briefly introduce two bacterial Raman datasets used in this paper in Section 2.1. Next, the structure of RamanNet is presented in Section 2.2. Then the experimental design of RamanNet will be described in Section 2.3.

2.1 Two bacterial Raman dataset

2.1.1 Bacteria-ID dataset. Our analysis was first conducted on the Bacteria-ID dataset published by Ho¹⁴ in 2019, the largest Raman dataset of pathogenic bacteria nowadays. We used its three isolated subsets: the reference, fine-tune, and test subsets, which are comprised of 2000, 100, and 100 spectra per isolate, respectively (Table 1). The dimension of all spectra in this dataset is 1000, and the isolates categories are 30. The test dataset is entirely independent of the reference and fine-tune subsets and gathered from separately cultured samples.

The wavenumber range of the spectra in all three datasets ranged from 381.98 to 1792.4 cm^{-1} . The spectral integration time in reference, fine-tuning, and test subsets are 1 s, 2 s, and 2 s, respectively. To keep the SNR (SNR = 4.1) consistent across

Table 1 A brief introduction to the Bacteria-ID dataset

	Spectral number	Measure time (s)	Isolates classes
Reference	60 000	1	30
Fine-tune	3000	2	30
Test	3000	2	30

datasets, for fine-tuning and test subsets, the integration time was increased from 1 s to 2 s due to the debasement of the optical system efficiency. The full isolate information and specific Raman experiment process obtained from the dataset were described in ref. 14, and the entire dataset was downloaded from <https://github.com/csho33/bacteria-ID/>.

2.1.2 PKU-bacterial dataset. We also tested RamanNet on another pathogenic bacterial dataset, the PKU-bacterial dataset, to demonstrate its robustness. The PKU-bacterial dataset was established by ourselves in 2022,¹⁵ which contains single-cell Raman spectra (scRS) of 15 pathogenic bacteria species. For each species, approximately 160 cells were isolated from three different patients; one patient's data were used as the test set, and the data from the other two patients were first augmented and then used as the training set.

The raw data of each scRS was pre-processed using home-made code, developed based on MATLAB (2021b) as follows: removing cosmic ray by median filtering, subtracting system background using polynomial baseline correction, smoothing with five-point smoothing, and normalizing by area. The normalized spectral data in the PKU-bacterial dataset has higher SNR than the Bacteria-ID dataset due to longer spectral integration time, exemplified by *S. epidermidis* (Fig. 1). The dimension of all spectra in this dataset is 861.

The details of the bacterial single-cell Raman spectroscopy measurement, data pre-processing, and data augmentation strategy were described in ref. 15.

2.2 Construction of RamanNet model

ResNet has enabled remarkable achievements in computer vision tasks. Compared to pictures with three-channel, machine

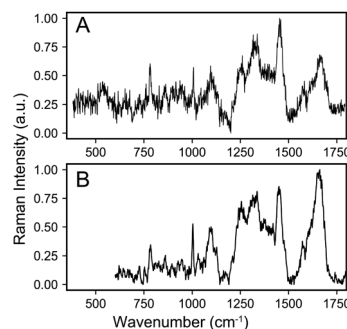


Fig. 1 A randomly selected spectrum of *S. epidermidis* from (A) Bacteria-ID dataset and (B) PKU-bacterial dataset. It can be seen that the SNR of the latter is higher than that of the former.



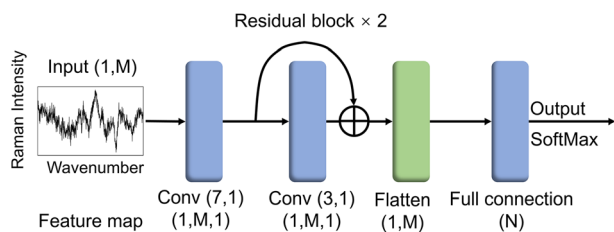


Fig. 2 Network of architectures of RamanNet for bacterial spectra classification. The layer structure, kernel size & number, and feature maps are listed in the diagrams. RamanNet model contains an initial convolution layer followed by two residual layers, a flatten layer, and a final fully connected classification layer. The residual block has an identity connection between the input and output of one convolutional layer. The feature map output by each layer is shown in the figure, where M represents the dimension of each spectrum, and N represents the bacterial classes. For the Bacteria-ID dataset, the M and N are 1000 and 30, respectively. For the PKU-bacterial dataset, M and N are 861 and 15, respectively.

vision (CV) commonly applied objects, the Raman spectrum is only one channel of digital sequence, and its data form is relatively simple. Given this characteristic of the Raman spectra, we simplified the classic ResNet¹⁹ structure and designed RamanNet.

The RamanNet consists of an initial convolution layer followed by two residual layers, a flatten layer, and a final fully connected classification layer (Fig. 2). Each residual layer contains a shortcut connection between the input and output of one convolutional layer, allowing for better gradient propagation and stable training.¹⁹ The convolution kernel numbers of all convolutional layers are set to 1. The size of the convolution kernel is 7 and 3, respectively. This simple model reduces traditional CNN's computational complexity so that it can be successfully trained on the Bacteria-ID dataset within 20 minutes, even on the CPU (Table 3). We adopted kaiming normal initialization²¹ and a “categorical_crossentropy” loss function. These architecture hyperparameters were selected *via* grid search using one training and validation split on the 30-isolates classification task.

2.3 Bacterial identification based on RamanNet and Raman spectra

2.3.1 Model training on Bacteria-ID dataset. We first trained the RamanNet network on the 30-isolate classification task, where the network's output is a probability vector of the 30 categories. The one with the largest probability was designed as

Table 3 Running time of ResNet on 30-isolates and 8-treatments tasks using CPU and GPU

Calculating unit	Pretraining (min)	Finetuning (min)	Prediction(s)
CPU (Intel i7-8700)	16.7	2.7	7.6
GPU (NVIDIA GeForce GTX 1080)	14.8	2.4	7.3

the predicted class. Binary MRSA/MSSA has the same architecture as the 30-isolated classifier, except for the number of categories in the final classification layer (Fig. 5).¹⁴ We first pre-trained RamanNet on the large-scale reference subset, then fine-tuned it on fine-tune subset to account for the degradation due to different Raman spectroscopy systems. The fine-tuning data were randomly split into five splits; each was divided into 9 : 1 as training and validation split, then trained the RamanNet on the training split and validated its accuracy on the validation split in order to perform model selection, thus five fine-tuned models were obtained. Finally, we evaluate and report the average test accuracy of these five fine-tuned models on the test subset gathered from independently cultured and prepared samples. In addition, the receiver operating characteristic (ROC) curve was used to verify the practicality of the ResNet model by plotting the true positive rate (TPR, sensitivity) *versus* the false-positive rate (FPR, 1-specificity) (Fig. 4).

In this work, we used the stochastic gradient descent (SGD) optimizer with a learning rate of 0.001 and a batch size of 10 to prevent overfitting, and early stopping technology was also used to avoid overfitting. Here pre-training was performed in only ten epochs; the fine-tuning was conducted in only 30 epochs.

2.3.2 Model training on PKU-bacterial dataset. To verify the robustness of our model, we also tested it on the PKU-bacterial dataset. Neural networks are data-driven models, so data augmentation is often used for neural network training^{22,23} to increase the dataset's diversity and enhance the model's generalization. Here the training set was randomly divided into training and validation subsets in a ratio of 9 : 1. The training subset is augmented with data, and the validation subset is not augmented. We adopted the following data augmentation strategies: (1) randomly shifted left or right a few wavenumbers, (2) added 1% Gaussian noise to the spectrum for each wavenumber, and (3) linearly combined all spectra from the same bacterial species, the combining coefficients are randomly generated so that we obtained the enhanced training subset for each species.

Table 2 Performance comparison between RamanNet and ResNet model¹⁴ on 30-isolates and 8-empiric-treatments identification task

Model	Accuracy			Parameters (mega)	Computation parameters (MACs)
	30-Isolates task	8-Treatments task	MRSA/MSSA		
RamanNet	84.7 ± 0.3%	97.1 ± 0.3%	81.6 ± 0.9%	0.030	0.03 M
ResNet ¹⁴	82.2 ± 0.3%	97.0 ± 0.3%	89.1 ± 0.1%	1.341	395 M



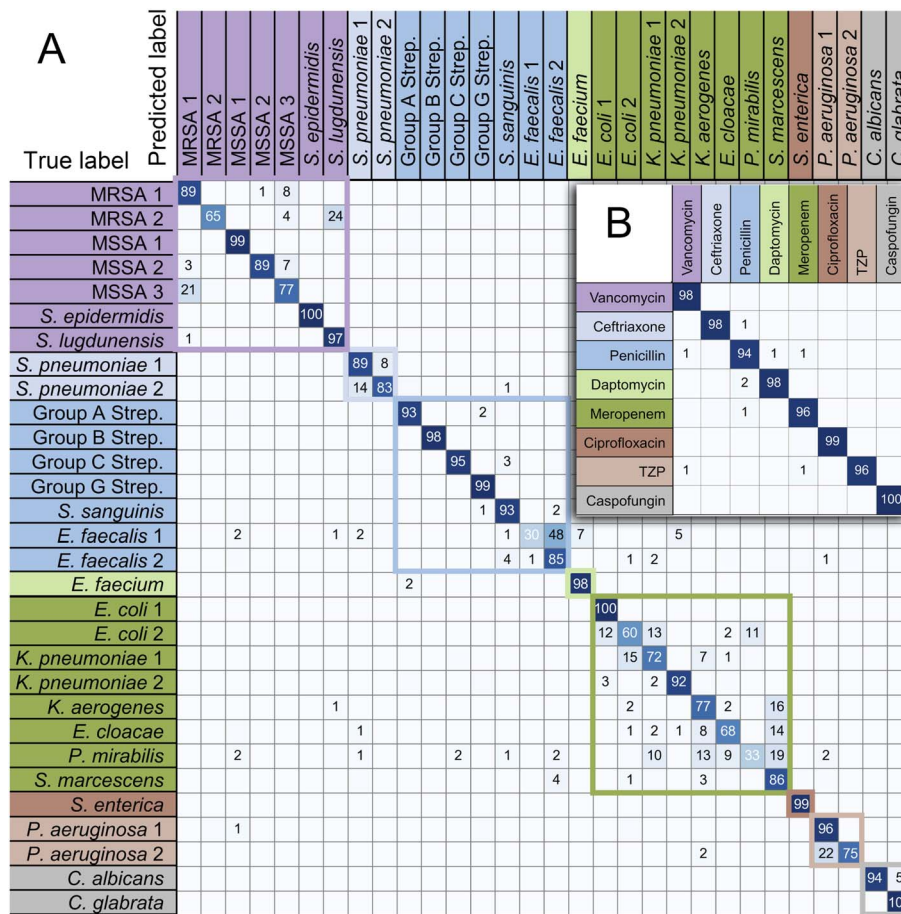


Fig. 3 RamanNet performance breakdown by class. The trained RamanNet classifies 30 bacterial and yeast isolates with (A) isolate-level accuracy of $84.7 \pm 0.3\%$ and (B) antibiotic grouping-level accuracy of $97.1 \pm 0.3\%$ (\pm calculated as standard deviation across five train and validation splits).

These training and validation processes were repeated on the training set five times to optimize the model. Finally, the model with the highest accuracy among the five optimized models acts

as the optimal trained model. Subsequently, we evaluated the accuracy of the optimal trained RamanNet model on the test set using the confusion matrix of 15 bacteria (Fig. 6), and the ROC curve (Fig. 7) was reported.

In this experiment, we use the SGD optimizer with a learning rate of 0.001 and a batch size of 6. The training was performed in 500 epochs, and early stopping technology was also used to prevent overfitting. If the accuracy on the validation subset does not rise for 100 consecutive epochs, the training process will end.

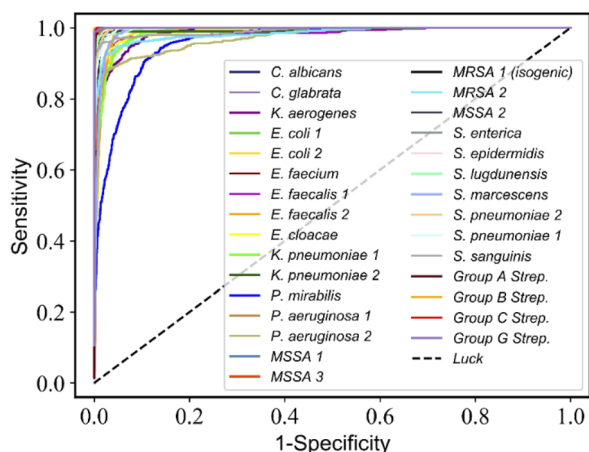


Fig. 4 ResNet discriminates the receiver operating characteristic (ROC) curve for 30-isolates Raman spectra. The average AUC values of 30 isolates are more than 0.98.

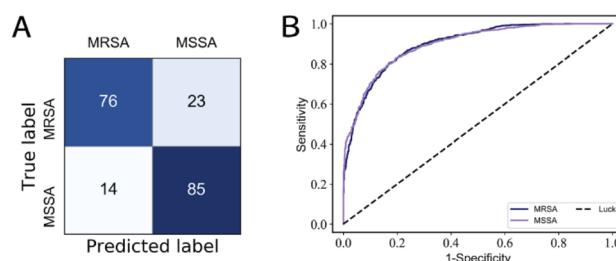


Fig. 5 (a) Confusion matrix of MSSA/MRSA; (b) ROC curve of MSSA/MRSA, the average AUC values are 0.90.



True label \ Predicted label	<i>S. marcescens</i>	<i>K. oxytoca</i>	<i>P. mirabilis</i>	<i>E. cloacae</i>	<i>P. aeruginosa</i>	<i>E. faecium</i>	<i>E. faecalis</i>	<i>C. amycolatum</i>	<i>S. haemolyticus</i>	<i>S. oralis</i>	<i>S. agalactiae</i>	<i>C. striatum</i>	<i>S. epidermidis</i>	<i>S. warneri</i>	<i>S. gordonii</i>
<i>S. marcescens</i>	100														
<i>K. oxytoca</i>	96	100								1	1				
<i>P. mirabilis</i>			100												
<i>E. cloacae</i>	1			96	1										
<i>P. aeruginosa</i>	4				95										
<i>E. faecium</i>						96	1		1						
<i>E. faecalis</i>						4	91	1		1	1				
<i>C. amycolatum</i>	3							90		1	1	1			
<i>S. haemolyticus</i>									96	1					1
<i>S. oralis</i>		1								96					
<i>S. agalactiae</i>											100				
<i>C. striatum</i>								3		5		90			
<i>S. epidermidis</i>									1	1			94	1	
<i>S. warneri</i>														98	
<i>S. gordonii</i>															100

Fig. 6 Confusion matrix for 15 bacterial species predicted by RamanNet. Blue represents Gram-negative bacteria, and red represents Gram-positive bacteria.

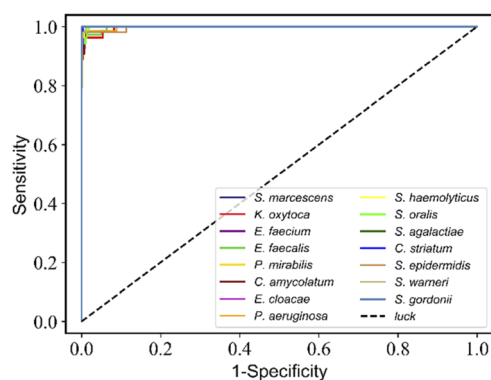


Fig. 7 RamanNet discriminates the receiver operating characteristic (ROC) curve for 15 species of bacterial scRS. The average AUC value of 15 species is more than 0.99.

3. Results and discussions

3.1 Classification performance of RamanNet on Bacteria-ID dataset

Recently, CNNs have been applied with tremendous success in various computer vision problems.^{14,24–26} And many deep models from image classification tasks have been directly used for spectral data. However, little work has been done to optimize those networks themselves based on spectral characteristics. In particular, most existing CNN-based Raman spectral classification work just changes the CNN model used for image classification to one-dimensional form and then directly was applied to Raman spectral classification task. Here, the architecture of RamanNet is greatly simplified (see Methods). Unlike previous work, the convolutional layer of RamanNet contains

only one convolution kernel, and the feature map has only one channel (Fig. 2). It does not need pooling layers and can preserve the exact locations of spectral peaks,¹⁴ thus significantly reducing the computational complexity. Benefiting from fewer model parameters, we demonstrated that RamanNet could be fast trained even using CPU without reducing significant training speed (Table 3).

Ibtehaz *et al.* proposed that the translational invariance of CNNs limits its application in Raman spectral classification, and used shifted multi-layer perceptions to simulate multi-layer convolutional layers to analyze shifted windows of Raman spectra.²⁷ We argue that the translational equivariance is provided by multiple convolutional operations and the global pooling operation. Here our proposed RamanNet only uses two convolutional layers and discards the global pooling operation through a single channel (each convolutional layer has only one convolution kernel), which greatly reduces the translation invariance and the model complexity.

On the 30-class task, the average isolate-level accuracy is $84.7 \pm 0.3\%$ (Fig. 3A). Gram-negative bacteria are primarily misclassified as other Gram-negative bacteria; the same is true for Gram-positive bacteria; most misclassifications occur within the same genus. For 30 isolates and MSSA/MRSA, the mean area under the ROC curve (AUC) value was over 0.98 (Fig. 4) and 0.90 (Fig. 5B), respectively.

The 8-empiric-treatments task determines whether the model can provide the correct recommended empiric treatment; here, the accuracy reaches $97.1 \pm 0.3\%$ (Fig. 3B).

As shown in Table 2, compared to ResNet,¹⁴ RamanNet achieves better accuracy on the 30-isolates task and similar results on the 8-treatments task, while the number of parameters was reduced to 0.030 M parameters (less by $44.7\times$), and the computational complexity (multiply-accumulate operations, MACs) was significantly reduced to 0.030 M MACs (less by $13\ 166.7\times$). Moreover, the training time of the RamanNet model was less than 20 minutes using CPU rather than GPU (Table 3). While, in distinguishing MRSA/MSSA, the identification accuracy of RamanNet was $81.6 \pm 0.9\%$ (Fig. 5A), lower than $89 \pm 0.9\%$ of ResNet (Table 2). This would be because they belong to the same species and are highly similar, so RamanNet may need further improvement in identifying bacterial subtypes. In brief, the above results demonstrated that RamanNet could achieve comparable or even better results at the species level than traditional ResNet on large Raman spectral datasets with low SNR. Thus, our model provides a quick and efficient way to analyze the Raman spectra of bacteria; it would be applied in the clinical diagnosis of bacterial diseases.

Table 4 Performance comparison between RamanNet and ResNet¹⁵ on 15-species identification in PKU-bacterial dataset

Model	Accuracy	Parameters (mega)	Computation parameters (MACs)
RamanNet	96.04%	0.013	0.013
ResNet	94.53%	3.86	9.64



3.2 Classification performance of RamanNet on PKU-bacterial dataset

For the 15-species bacteria of the PKU-bacterial dataset, the average identification accuracy of RamanNet models on the test set reaches 96.04% (Table 4), which is better than 94.53% of ResNet. From the confusion matrix (Fig. 6), we can see that the identification accuracy was over 93% for the 12 of 15 bacteria and over 89% for 15 of 15 bacteria. Generally, Gram-positive bacteria are misclassified as other Gram-positive bacteria, and Gram-negative bacteria are the same. In addition, the specificity and sensitivity of the RamanNet model were also evaluated by ROC (Fig. 7). For all 15 species, the mean value of AUC (the areas under the ROC curves) is over 0.99.

4. Conclusion

In the information age, deep learning of convolutional neural networks is widely used in many fields. Bacterial identification based on Raman spectroscopy is also booming, thanks to the development of artificial intelligence. In this work, we have developed a new simple convolutional network model (RamanNet) with a few model parameters for rapid and accurate classification of the Raman spectrum of a single bacterium. The model has been evaluated on both an open lower SNR bigger bacterial Raman spectral dataset (the Bacteria-ID dataset) and self-developed small but higher SNR bacterial Raman spectral datasets (PKU-bacterial dataset). The results show RamanNet has higher (or comparable) accuracy than the popular ResNet model. Moreover, we can use the CPU to train the RamanNet model and eliminate the limitation of GPU without sacrificing significant speed. Therefore, our model promotes Raman spectroscopy-based bacterial identification and has a potential in other scRS-based Cells classification tasks.

Author contributions

Bo Zhou proposed the idea of optimizing the neural network model, trained and optimized models, and led the writing of the manuscript. Anpei Ye funded this research, constructed the optical tweezers system, helped analyze the results, and revised the thesis. Ru Zhang funded this research and oversaw the project with Anpei Ye together. Yu-Kai Tong participated in the discussion of model optimization.

Conflicts of interest

There are no conflicts to declare.

Acknowledgements

This work was supported by the National Natural Science Foundation of China (NSFC) (U19A2007, 32150026, 92043302, 61671085). Bo Zhou thanks Zheng Li of the Beijing University of Posts and Telecommunications for valuable discussions. We thank Chi-Sing Ho *et al.* for providing the publicly available Bacterial-ID dataset so that we can use it for algorithm

optimization research. We thank Haixia Li and Prof. Liying Sun from Peking University First Hospital for providing clinical bacteria that allowed us to build a single-cell Raman spectral database with high SNR.

Notes and references

- 1 B. Swaminathan and P. Feng, *Annu. Rev. Microbiol.*, 1994, **48**, 401–426.
- 2 S. M. Hamlet, in *Oral Biology*, Springer, 2010, pp. 125–140.
- 3 K. L. Josephson, C. P. Gerba and I. L. Pepper, *Appl. Environ. Microbiol.*, 1993, **59**, 3513–3515.
- 4 S. S. Han, Y. S. Jeong and S. K. Choi, *Microorganisms*, 2021, **9**, 1917.
- 5 C. Papagiannopoulou, R. Parchen, P. Rubbens and W. Waegeman, *Anal. Chem.*, 2020, **92**, 7523–7531.
- 6 Y. Dai, C. Li, J. Yi, Q. Qin, B. Liu and L. Qiao, *Anal. Chem.*, 2020, **92**, 8051–8057.
- 7 J. Dietvorst, L. Vilaplana, N. Uria, M.-P. Marco and X. Muñoz-Berbel, *TrAC, Trends Anal. Chem.*, 2020, **127**, 115891.
- 8 J. Zhu, A. S. Sharma, J. Xu, Y. Xu, T. Jiao, Q. Ouyang, H. Li and Q. Chen, *Spectrochim. Acta, Part A*, 2021, **246**, 118994.
- 9 S. Yan, S. Wang, J. Qiu, M. Li, D. Li, D. Xu, D. Li and Q. Liu, *Talanta*, 2021, **226**, 122195.
- 10 L. Deng, Y. Zhong, M. Wang, X. Zheng and J. Zhang, *IEEE J. Biomed. Health Inform.*, 2021, **26**, 369–378.
- 11 W. Lu, X. Chen, L. Wang, H. Li and Y. V. Fu, *Anal. Chem.*, 2020, **92**, 6288–6296.
- 12 L. Pan, P. Zhang, C. Daengngam, S. Peng and M. Chongcheawchamnan, *J. Raman Spectrosc.*, 2022, **53**, 6–19.
- 13 K. Y. Noonan, L. A. Tonge, O. S. Fenton, D. B. Damiano and K. A. Frederick, *Appl. Spectrosc.*, 2009, **63**, 742–747.
- 14 C. S. Ho, N. Jean, C. A. Hogan, L. Blackmon, S. S. Jeffrey, M. Holodniy, N. Banaei, A. A. E. Saleh, S. Ermon and J. Dionne, *Nat. Commun.*, 2019, **10**, 4927.
- 15 B. Zhou, L. Sun, T. Fang, H. Li, R. Zhang and A. Ye, *J. Biophotonics*, 2022, e202100312.
- 16 M. K. Maruthamuthu, A. H. Raffiee, D. M. De Oliveira, A. M. Ardekani and M. S. Verma, *Microbiologyopen*, 2020, **9**, e1122.
- 17 X. Zhang, J. Xu, J. Yang, L. Chen, H. Zhou, X. Liu, H. Li, T. Lin and Y. Ying, *Anal. Chim. Acta*, 2020, **1119**, 41–51.
- 18 S. Weng, H. Yuan, X. Zhang, P. Li, L. Zheng, J. Zhao and L. Huang, *Analyst*, 2020, **145**, 4827–4835.
- 19 K. He, X. Zhang, S. Ren and J. Sun, in *Proceedings of the IEEE conference on computer vision and pattern recognition*, 2016, pp. 770–778.
- 20 Y. Liu, J. Xu, Y. Tao, T. Fang, W. Du and A. Ye, *Analyst*, 2020, **145**, 3297–3305.
- 21 K. He, X. Zhang, S. Ren, J. Sun, *IEEE International Conference on Computer Vision*, 2015, pp. 1026–1034, DOI: [10.1109/iccv.2015.123](https://doi.org/10.1109/iccv.2015.123).
- 22 H. He, S. Yan, D. Lyu, M. Xu, R. Ye, P. Zheng, X. Lu, L. Wang and B. Ren, *Anal. Chem.*, 2021, **93**, 3653–3665.
- 23 P. Pradhan, S. Guo, O. Ryabchykov, J. Popp and T. W. Bocklitz, *J. Biophotonics*, 2020, **13**, e201960186.



- 24 L. Liu, W. Ouyang, X. Wang, P. Fieguth, J. Chen, X. Liu and M. Pietikäinen, *Int. J. Comput. Vis.*, 2019, **128**, 261–318.
- 25 Y. Sun, B. Xue, M. Zhang, G. G. Yen and J. Lv, *IEEE Trans. Cybern.*, 2020, **50**, 3840–3854.
- 26 G. W. Lindsay, *J. Cogn. Neurosci.*, 2021, **33**, 2017–2031.
- 27 N. Ibtehaz, M. E. H. Chowdhury, A. Khandakar, S. M. Zughaier, S. Kiranyaz, and M. Sohel Rahman, 2022, arXiv:2201.09737 [cs.LG].

